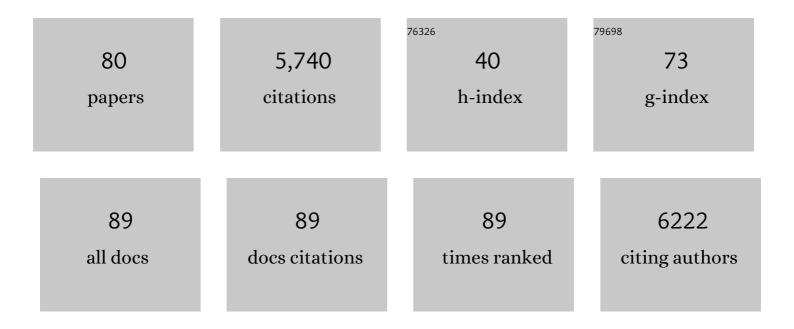
List of Publications by Year in descending order

Source: https://exaly.com/author-pdf/2362674/publications.pdf Version: 2024-02-01



<u> Ρετέρ Νορτή</u>

#	Article	IF	CITATIONS
1	Amazon forests maintain consistent canopy structure and greenness during the dry season. Nature, 2014, 506, 221-224.	27.8	354
2	Remote sensing of canopy light use efficiency using the photochemical reflectance index. Remote Sensing of Environment, 2001, 78, 264-273.	11.0	278
3	Quantifying Vegetation Biophysical Variables from Imaging Spectroscopy Data: A Review on Retrieval Methods. Surveys in Geophysics, 2019, 40, 589-629.	4.6	265
4	Three-dimensional forest light interaction model using a Monte Carlo method. IEEE Transactions on Geoscience and Remote Sensing, 1996, 34, 946-956.	6.3	261
5	The impact of diffuse sunlight on canopy lightâ€use efficiency, gross photosynthetic product and net ecosystem exchange in three forest biomes. Global Change Biology, 2007, 13, 776-787.	9.5	222
6	Previsual symptoms of Xylella fastidiosa infection revealed in spectral plant-trait alterations. Nature Plants, 2018, 4, 432-439.	9.3	212
7	Aerosol remote sensing over land: A comparison of satellite retrievals using different algorithms and instruments. Atmospheric Research, 2007, 85, 372-394.	4.1	196
8	Third Radiation Transfer Model Intercomparison (RAMI) exercise: Documenting progress in canopy reflectance models. Journal of Geophysical Research, 2007, 112, .	3.3	193
9	Control of atmospheric particles on diffuse radiation and terrestrial plant productivity. Progress in Physical Geography, 2012, 36, 209-237.	3.2	177
10	The Propagation of Foliar Biochemical Absorption Features in Forest Canopy Reflectance. Remote Sensing of Environment, 1999, 67, 147-159.	11.0	144
11	Radiation transfer model intercomparison (RAMI) exercise. Journal of Geophysical Research, 2001, 106, 11937-11956.	3.3	138
12	Analyzing the effect of structural variability and canopy gaps on forest BRDF using a geometric-optical model. Remote Sensing of Environment, 1997, 62, 46-62.	11.0	137
13	The inter-comparison of major satellite aerosol retrieval algorithms using simulated intensity and polarization characteristics of reflected light. Atmospheric Measurement Techniques, 2010, 3, 909-932.	3.1	136
14	Radiation Transfer Model Intercomparison (RAMI) exercise: Results from the second phase. Journal of Geophysical Research, 2004, 109, n/a-n/a.	3.3	131
15	Development, Production and Evaluation of Aerosol Climate Data Records from European Satellite Observations (Aerosol_cci). Remote Sensing, 2016, 8, 421.	4.0	131
16	Vegetation height estimates for a mixed temperate forest using satellite laser altimetry. International Journal of Remote Sensing, 2008, 29, 1475-1493.	2.9	124
17	Monte Carlo ray tracing in optical canopy reflectance modelling. International Journal of Remote Sensing, 2000, 18, 163-196.	1.0	117
18	Evaluation of seven European aerosol optical depth retrieval algorithms for climate analysis. Remote Sensing of Environment, 2015, 162, 295-315.	11.0	112

#	Article	IF	CITATIONS
19	Retrieval of land surface bidirectional reflectance and aerosol opacity from ATSR-2 multiangle imagery. IEEE Transactions on Geoscience and Remote Sensing, 1999, 37, 526-537.	6.3	109
20	Merging regional and global aerosol optical depth records from major available satellite products. Atmospheric Chemistry and Physics, 2020, 20, 2031-2056.	4.9	98
21	Estimation of fAPAR, LAI, and vegetation fractional cover from ATSR-2 imagery. Remote Sensing of Environment, 2002, 80, 114-121.	11.0	96
22	AeroCom phase III multi-model evaluation of the aerosol life cycle and optical properties using ground- and space-based remote sensing as well as surface in situ observations. Atmospheric Chemistry and Physics, 2021, 21, 87-128.	4.9	96
23	Vegetation height and cover fraction between 60° S and 60° N from ICESat GLAS data. Geoscientific Model Development, 2012, 5, 413-432.	3.6	94
24	Assessing the effects of forest health on sun-induced chlorophyll fluorescence using the FluorFLIGHT 3-D radiative transfer model to account for forest structure. Remote Sensing of Environment, 2017, 193, 165-179.	11.0	94
25	Aerosol optical depth and land surface reflectance from multiangle AATSR measurements: global validation and intersensor comparisons. IEEE Transactions on Geoscience and Remote Sensing, 2006, 44, 2184-2197.	6.3	90
26	New Vegetation Albedo Parameters and Global Fields of Soil Background Albedo Derived from MODIS for Use in a Climate Model. Journal of Hydrometeorology, 2009, 10, 183-198.	1.9	87
27	The RAMI On-line Model Checker (ROMC): A web-based benchmarking facility for canopy reflectance models. Remote Sensing of Environment, 2008, 112, 1144-1150.	11.0	85
28	A method to convert AVHRR Normalized Difference Vegetation Index time series to a standard viewing and illumination geometry. Remote Sensing of Environment, 2005, 99, 400-411.	11.0	84
29	Aerosol retrieval experiments in the ESA Aerosol_cci project. Atmospheric Measurement Techniques, 2013, 6, 1919-1957.	3.1	76
30	Estimation of aerosol opacity and land surface bidirectional reflectance from ATSR-2 dual-angle imagery: Operational method and validation. Journal of Geophysical Research, 2002, 107, AAC 4-1.	3.3	75
31	Forest ecosystem chlorophyll content: Implications for remotely sensed estimates of net primary productivity. International Journal of Remote Sensing, 2003, 24, 611-617.	2.9	74
32	A Monte Carlo radiative transfer model of satellite waveform LiDAR. International Journal of Remote Sensing, 2010, 31, 1343-1358.	2.9	73
33	Impact of atmospheric aerosol from biomass burning on Amazon dryâ€season drought. Journal of Geophysical Research, 2009, 114, .	3.3	71
34	A global dataset of atmospheric aerosol optical depth and surface reflectance from AATSR. Remote Sensing of Environment, 2012, 116, 199-210.	11.0	66
35	An observation-based estimate of the strength of rainfall-vegetation interactions in the Sahel. Geophysical Research Letters, 2006, 33, .	4.0	63
36	Mapping radiation interception in row-structured orchards using 3D simulation and high-resolution airborne imagery acquired from a UAV. Precision Agriculture, 2012, 13, 473-500.	6.0	62

#	Article	IF	CITATIONS
37	Improved global simulations of gross primary product based on a separate and explicit treatment of diffuse and direct sunlight. Journal of Geophysical Research, 2007, 112, .	3.3	51
38	Synergistic use of MERIS and AATSR as a proxy for estimating Land Surface Temperature from Sentinel-3 data. Remote Sensing of Environment, 2016, 179, 149-161.	11.0	49
39	Monitoring the incidence of Xylella fastidiosa infection in olive orchards using ground-based evaluations, airborne imaging spectroscopy and Sentinel-2 time series through 3-D radiative transfer modelling. Remote Sensing of Environment, 2020, 236, 111480.	11.0	49
40	The uncertainty of biomass estimates from modeled ICESat-2 returns across a boreal forest gradient. Remote Sensing of Environment, 2015, 158, 95-109.	11.0	47
41	Computationally efficient method for retrieving aerosol optical depth from ATSR-2 and AATSR data. Applied Optics, 2006, 45, 2786.	2.1	42
42	Uncertainty within satellite LiDAR estimations of vegetation and topography. International Journal of Remote Sensing, 2010, 31, 1325-1342.	2.9	40
43	An AeroCom–AeroSat study: intercomparison of satellite AOD datasets for aerosol model evaluation. Atmospheric Chemistry and Physics, 2020, 20, 12431-12457.	4.9	40
44	Satellite-driven modelling of Net Primary Productivity (NPP): Theoretical analysis. Remote Sensing of Environment, 2009, 113, 137-147.	11.0	39
45	Intercomparison of desert dust optical depth from satellite measurements. Atmospheric Measurement Techniques, 2012, 5, 1973-2002.	3.1	37
46	Radiative transfer modeling of direct and diffuse sunlight in a Siberian pine forest. Journal of Geophysical Research, 2005, 110, .	3.3	36
47	A sensitivity analysis of the land-surface scheme JULES conducted for three forest biomes: Biophysical parameters, model processes, and meteorological driving data. Global Biogeochemical Cycles, 2006, 20, n/a-n/a.	4.9	32
48	Model inversion for chlorophyll estimation in open canopies from hyperspectral imagery. International Journal of Remote Sensing, 2008, 29, 5093-5111.	2.9	30
49	Ground and Top of Canopy Extraction From Photon-Counting LiDAR Data Using Local Outlier Factor With Ellipse Searching Area. IEEE Geoscience and Remote Sensing Letters, 2019, 16, 1447-1451.	3.1	29
50	Statistical Distances and Their Applications to Biophysical Parameter Estimation: Information Measures, M-Estimates, and Minimum Contrast Methods. Remote Sensing, 2013, 5, 1355-1388.	4.0	27
51	Estimating forest canopy parameters from satellite waveform LiDAR by inversion of the FLIGHT three-dimensional radiative transfer model. Remote Sensing of Environment, 2017, 188, 177-189.	11.0	25
52	Smoke aerosol properties and ageing effects for northern temperate and boreal regions derived from AERONET source and age attribution. Atmospheric Chemistry and Physics, 2015, 15, 7929-7943.	4.9	24
53	Improving the Performance of 3-D Radiative Transfer Model FLICHT to Simulate Optical Properties of a Tree-Grass Ecosystem. Remote Sensing, 2018, 10, 2061.	4.0	24
54	Slope Estimation from ICESat/GLAS. Remote Sensing, 2014, 6, 10051-10069.	4.0	23

#	Article	IF	CITATIONS
55	Particulate emissions from large North American wildfires estimated using a new top-down method. Atmospheric Chemistry and Physics, 2017, 17, 6423-6438.	4.9	21
56	Interpreting shallow, vertical nitrogen profiles in tree crowns: A three-dimensional, radiative-transfer simulation accounting for diffuse sunlight. Agricultural and Forest Meteorology, 2007, 145, 110-124.	4.8	19
57	The inter-comparison of AATSR dual-view aerosol optical thickness retrievals with results from various algorithms and instruments. International Journal of Remote Sensing, 2009, 30, 4525-4537.	2.9	19
58	A comparison of biophysical parameter retrieval for forestry using airborne and satellite LiDAR. International Journal of Remote Sensing, 2009, 30, 5229-5237.	2.9	18
59	Improvements in Aerosol Optical Depth Estimation Using Multiangle CHRIS/PROBA Images. IEEE Transactions on Geoscience and Remote Sensing, 2010, 48, 18-24.	6.3	18
60	Potential of Forest Parameter Estimation Using Metrics from Photon Counting LiDAR Data in Howland Research Forest. Remote Sensing, 2019, 11, 856.	4.0	18
61	Response of vegetation to the 2003 European drought was mitigated by height. Biogeosciences, 2014, 11, 2897-2908.	3.3	17
62	Stratospheric aerosol radiative forcing simulated by the chemistry climate model EMAC using Aerosol CCI satellite data. Atmospheric Chemistry and Physics, 2018, 18, 12845-12857.	4.9	17
63	Retrieval of leaf area index from MODIS surface reflectance by model inversion using different minimization criteria. Remote Sensing of Environment, 2013, 139, 257-270.	11.0	15
64	Uncertainty in Aerosol Optical Depth From Modern Aerosolâ€Climate Models, Reanalyses, and Satellite Products. Journal of Geophysical Research D: Atmospheres, 2022, 127, .	3.3	15
65	Evaluating Prospects for Improved Forest Parameter Retrieval From Satellite LiDAR Using a Physically-Based Radiative Transfer Model. IEEE Journal of Selected Topics in Applied Earth Observations and Remote Sensing, 2013, 6, 45-53.	4.9	13
66	Evaluating the potential of LiDAR data for fire damage assessment: A radiative transfer model approach. Remote Sensing of Environment, 2020, 247, 111893.	11.0	13
67	The ESA globAlbedo project: Algorithm. , 2012, , .		11
68	Synergistic angular and spectral estimation of aerosol properties using CHRIS/PROBA-1 and simulated Sentinel-3 data. Atmospheric Measurement Techniques, 2015, 8, 1719-1731.	3.1	8
69	Forestry Applications for Satellite Lidar Remote Sensing. Photogrammetric Engineering and Remote Sensing, 2011, 77, 271-279.	0.6	7
70	New data sets for climate change and land use studies are on track. Eos, 1999, 80, 589.	0.1	6
71	Forest signal detection for photon counting LiDAR using Random Forest. Remote Sensing Letters, 2020, 11, 37-46.	1.4	6
72	Validation of Aerosol Products from AATSR and MERIS/AATSR Synergy Algorithms—Part 1: Global Evaluation. Remote Sensing, 2018, 10, 1414.	4.0	5

#	Article	IF	CITATIONS
73	Morton et al. reply. Nature, 2016, 531, E6-E6.	27.8	2
74	Dual-view operational atmospheric correction for ATSR-2 imagery. , 1998, , .		1
75	Global atmospheric aerosol optical depth retrievals over land and ocean from AATSR. , 2009, , .		1
76	Quantitative global mapping of terrestrial vegetation photosynthesis: The Fluorescence Explorer (FLEX) mission. , 2017, , .		1
77	Stemwood Volume Estimates for a Mixed Temperate Forest using Satellite LiDAR(<special) 0.784314<="" 1="" etqq1="" td="" tj=""><td>rgBT /Ov</td><td>erlock 10 Tf</td></special)>	rgBT /Ov	erlock 10 Tf
78	NATURAL RESOURCE IN SOUTHERN AFRICAN DRYLANDS: DETERMINING SPATIAL AVAILABILITY AND VARIABILITY USING ATSR2 TIME SERIES. , 2002, , .		0
79	Simulation and assessment of hyperspectral imagery. , 2004, , .		0
80	Monitoring Forest Health with Sun-Induced Chlorophyll Fluorescence Observations and 3-D Radiative Transfer Modeling. , 2018, , .		0